MARINE SCIENCE

Kīlauea lava fuels phytoplankton bloom in the North Pacific Ocean

Samuel T. Wilson[1*†], Nicholas J. Hawco[2*†], E. Virginia Armbrust[3], Benedetto Barone[1], Karin M. Björkman[1], Angela K. Boysen[3], Macarena Burgos[1], Timothy J. Burrell[1], John R. Casey[1,4], Edward F. DeLong[1], Mathilde Dugenne[1], Stephanie Dutkiewicz[4], Sonya T. Dyhrman[5,6], Sara Ferrón[1], Michael J. Follows[4], Rhea K. Foreman[1], Carolina P. Funkey[1], Matthew J. Harke[6], Britt A. Henke[7], Christopher N. Hill[4], Annette M. Hynes[3], Anitra E. Ingalls[3], Oliver Jahn[4], Rachel L. Kelly[2], Angela N. Knapp[8], Ricardo M. Letelier[9], Francois Ribalet[3], Eric M. Shimabukuro[1], Ryan K. S. Tabata[1], Kendra A. Turk-Kubo[7], Angelicque E. White[1], Jonathan P. Zehr[7], Seth John[2], David M. Karl[1]

From June to August 2018, the eruption of Kīlauea volcano on the island of Hawai'i injected millions of cubic meters of molten lava into the nutrient-poor waters of the North Pacific Subtropical Gyre. The lava-impacted seawater was characterized by high concentrations of metals and nutrients that stimulated phytoplankton growth, resulting in an extensive plume of chlorophyll a that was detectable by satellite. Chemical and molecular evidence revealed that this biological response hinged on unexpectedly high concentrations of nitrate, despite the negligible quantities of nitrogen in basaltic lava. We hypothesize that the high nitrate was caused by buoyant plumes of nutrient-rich deep waters created by the substantial input of lava into the ocean. This large-scale ocean fertilization was therefore a unique perturbation event that revealed how marine ecosystems respond to exogenous inputs of nutrients.

One of the most active volcanoes in the world, Kīlauea on the island of Hawai'i, erupted from April to August 2018. The eruption produced an extensive channel of molten lava that flowed into the ocean at an estimated rate of 50 to 100 $m^3\ s^{-1}$ for 2 months, from 3 June 2018 until 6 August 2018, ultimately creating an additional 3.5 km^2 of coastal area (*1*, *2*). Three days after lava first entered the ocean, high chlorophyll a concentrations were observed in the vicinity by the MODIS Aqua satellite (Fig. 1). Chlorophyll a–enriched waters rapidly expanded in size and within 2 weeks had extended 150 km offshore as a highly prominent filament. To understand the trajectory of the chlorophyll a plume, a numerical simulation was run in which dye was continuously released at the lava ocean entry site into a flow field estimated from winds and pressure gradients at the sea surface. The results of the simulation indicated that the trajectory of the chlorophyll a filament was dictated by the surface flow field associated with the edge of a cyclonic eddy located to the northeast of Hawai'i (Fig. 1). Chlorophyll a concentrations within this filament remained elevated (>0.2 μg chl a $liter^{-1}$) throughout the eruption period and exceeded values observed in this region during the past 15 years (fig. S1). Once the lava flow subsided on 6 August 2018, the chlorophyll a filament subsequently dissipated within a week, indicating that volcanic processes were directly responsible for the observed phytoplankton bloom. Therefore, the spatial distribution of the chlorophyll a filament was used to delineate the extent of lava-impacted waters.

During peak discharge of lava into the ocean (Fig. 1), an oceanographic research expedition was conducted to determine the causes and composition of the resulting phytoplankton bloom (fig. S2). In contrast to the surrounding homogeneous oligotrophic ocean, chlorophyll a concentrations within the lava-impacted plume waters were highly variable, ranging from 0.1 to 0.6 μg chl a $liter^{-1}$ near the lava entry site (Fig. 1). The plume also contained elevated concentrations of trace metals, rare earth elements, inorganic nutrients, and particulate material. Within the plume, surface seawater concentrations of silicic acid and trace metals including manganese, iron, and cobalt strongly resembled the composition of Kīlauea reference basalt material (*3*, *4*) (fig. S3). The solubility of these metals differed markedly. For example, >99% of manganese remained in the dissolved phase (<0.2 μm size fraction) while >99% of iron had precipitated (data S1). Similar to deep-sea hydrothermal vent environments (*5*), the micromolar levels of iron oxyhydroxide particles promoted the scavenging of rare earth elements and phosphate, thereby causing only a slight enrichment of dissolved phosphate within the plume. The scavenging onto particles also likely contributed to the observed elevated concentrations of particulate phosphorus (table S1). Surprisingly, given the lack of fixed nitrogen species in mantle-derived magmas (*6*), surface plume waters contained up to 4 μmol $liter^{-1}$ nitrate, significantly higher than background concentrations in the surrounding oligotrophic waters (<0.01 μmol $liter^{-1}$; table S1). To examine the fate of nutrients at the broader scale, we used a biogeochemical model embedded within a high-resolution regional physical flow field (fig. S4). The modeled input of silicic acid, iron, nitrate, and phosphate along the southeast coast of Hawai'i was sufficient to simulate a phytoplankton bloom both near the lava entry site and hundreds of kilometers downstream, sustained from the recycling of lava-associated nutrients (see supplementary text).

The shipboard observations of the transition zone between lava-impacted plume waters and the ambient oligotrophic ocean revealed steep biogeochemical gradients, with silicic acid, nitrate, metals, and chlorophyll decreasing from peak values to typical background oligotrophic ocean concentrations over a distance of approximately 2 km (Fig. 2). To further investigate the lava-impacted waters and the transition zone, particularly in regard to subsurface features, an autonomous SeaGlider conducted vertical profiles in the vicinity (fig. S5). The SeaGlider identified several maxima in chlorophyll a concentrations located just beneath the mixed layer, which varied between depths of 5 to 50 m in the water column (fig. S6B). Coincident high values of particle backscatter at these depths (fig. S6C) helped distinguish these near-surface chlorophyll maxima from the deep chlorophyll maxima that are typical of stratified oligotrophic regions, which are due to changes in the phytoplankton chlorophyll:carbon ratios rather than to phytoplankton biomass (*7*).

Within the lava-impacted waters, plankton carbon biomass [based on measurements of carbon per unit biovolume (*8*) (see supplementary text)] increased by a factor of 2 to 3 relative to surrounding oligotrophic waters, and primarily comprised large chain-forming diatoms in the genus *Skeletonema* (37% of estimated total carbon biomass; Fig. 3, A and B). *Skeletonema* sp. are commonly found in coastal waters of the Hawaiian Islands, and their strong response to lava input reflects a combination of their initial population size and intrinsic traits that allow them to capitalize on the nutrient inputs associated with lava (*9*). Accompanying the increases in diatom abundance was an increase in zooplankton nauplii (11% of total biomass) as well as other phytoplankton, such as haptophytes (represented

[1]Department of Oceanography, Daniel K. Inouye Center for Microbial Oceanography: Research and Education (C-MORE), University of Hawai'i at Manoa, Honolulu, HI 96822, USA. [2]Department of Earth Sciences, University of Southern California, Los Angeles, CA 90089, USA. [3]School of Oceanography, University of Washington, Seattle, WA 98195, USA. [4]Department of Earth, Atmospheric, and Planetary Sciences, Massachusetts Institute of Technology, Cambridge, MA 02139, USA. [5]Department of Earth and Environmental Sciences, Columbia University, Palisades, NY 10964, USA. [6]Lamont-Doherty Earth Observatory, Columbia University, Palisades, NY 10964, USA. [7]Department of Ocean Sciences, University of California, Santa Cruz, CA 95064, USA. [8]Department of Earth, Ocean, and Atmospheric Science, Florida State University, Tallahassee, FL 32306, USA. [9]College of Earth, Ocean, and Atmospheric Sciences, Oregon State University, Corvallis, OR 97331, USA.
***Corresponding author. Email: stwilson@hawaii.edu (S.T.W.); hawco@usc.edu (N.J.H.)** †These authors contributed equally to this work.

primarily by *Phaeocystis*) and radiolarians (represented primarily by *Sphaeropylolena*). Although large microorganisms dominated the plankton biomass, the typical oligotrophic phytoplankton community of *Prochlorococcus*, *Synechococcus*, and picoeukaryotes remained numerically abundant and together represented 18% of estimated total carbon biomass. The coexistence of diatoms and *Prochlorococcus* supports the hypothesis that the increase in diatom biomass in response to nutrient inputs in the open ocean does not lessen abundant nano- and picophytoplankton populations (*10*). Highly elevated rates of biological production were detected within the plume waters. Rates of ^{14}C-bicarbonate assimilation ranged from 2.5 to 3.5 μmol C liter^{-1} day^{-1} (compared to 0.5 to 0.6 μmol C liter^{-1} day^{-1} in ambient oligotrophic waters), and gross primary production based on the ^{18}O-H_2O method ranged from 4 to 6 μmol O_2 liter^{-1} day^{-1} (compared to 0.9 to 1.1 μmol O_2 liter^{-1} day^{-1} in ambient oligotrophic waters) (fig. S7). At the most near-shore sampling station, the high rates of biological production coincided with high rates of microbial respiration that reached 5.1 ± 0.6 μmol O_2 liter^{-1} day^{-1} (mean ± SD; fig. S7).

Surprisingly, the lava-impacted waters did not support an abundance of diazotrophs, nor did they lead to high rates of nitrogen fixation (fig. S7) despite the presence of sufficient amounts of iron and phosphorus expected to enhance biological nitrogen fixation (*11*, *12*). Instead, the metabolic response to lava-impacted waters indicated that nitrate, rather than biological nitrogen fixation, was the key driver of the observed phytoplankton bloom. Detailed analysis of functional gene responses specific to diatoms in the lava-impacted waters relative to surrounding water revealed significant increases in relative transcript abundance for genes associated with growth processes such as ribosomal biogenesis, photosynthesis, and adenosine triphosphate synthesis, whereas decreases were detected in relative transcript abundance for genes involved in the assimilation of nitrogen (fig. S8F). These results are consistent with prior observations of relief from nitrogen limitation in diatoms (*9*, *13*, *14*). Shifts in relative transcript abundance specific to *Skeletonema* largely mirrored those observed in the whole diatom community (fig. S8G). Within the plume, *Skeletonema* genes involved in the assimilation of nitrogen, including those that encode nitrate and ammonium transporters, nitrate reductase, and glutamate synthase, showed significant decreases in relative transcript abundance, whereas significant increases in relative transcript abundance were observed for genes involved in photosynthesis (*psbA*, *psbC*) and carbon fixation (*rbcS*, *rbcL*) (Fig. 3C). The relative abundance of *Skeletonema* transcripts related to iron transport decreased in the lava-impacted waters (Fig. 3C), consistent with the high concentrations of iron within the plume (data S3).

The composition and physiology of the phytoplankton within the plume therefore suggested that nitrate availability was a key component of the phytoplankton bloom. We confirmed this hypothesis by determining the isotopic composition of suspended particulate nitrogen (δ^{15}N-PN) and nitrate (δ^{15}N-NO_3^- and δ^{18}O-NO_3^-) within the plume. The δ^{15}N-PN signature ranged from 4.5 to 4.8 per mil (‰), whereas a δ^{15}N signature closer to 0‰ would have represented a larger contribution from biological nitrogen fixation. Moreover, the δ^{15}N-PN values were ~5‰ lower than the δ^{15}N-NO_3^- within the lava-impacted plume waters, with δ^{15}N-NO_3^- values of 9.4 ± 1.3‰ and δ^{18}O-NO_3^- values of 7.0 ± 1.6‰ (mean ± SD, n = 16). This is consistent with the magnitude of isotopic fractionation previously observed in phytoplankton cultures (*15*). The nearly 1:1 correlation observed between δ^{15}N-NO_3^- and δ^{18}O-NO_3^- in lava-impacted waters (Fig. 4A) is an additional signature of biological nitrate uptake. Thus, molecular and isotopic markers of phytoplankton nitrogen utilization are consistent with nitrate supporting the elevated phytoplankton biomass in the lava-impacted waters.

Although there was clear evidence for the biological importance of high nitrate concentrations in lava-impacted waters, the pathway of

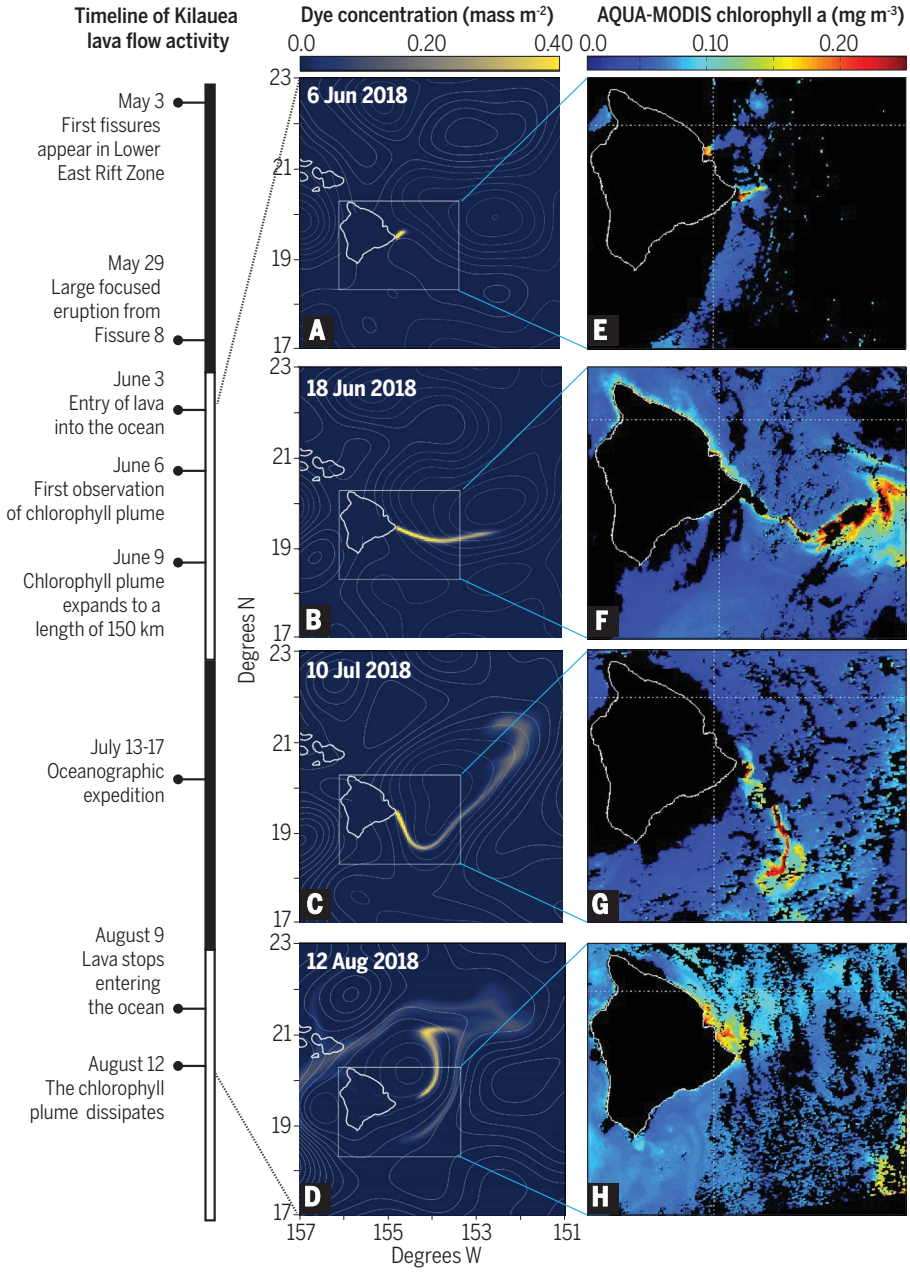

Fig. 1. Timeline of Kīlauea eruptive activity focusing on events related to lava entering the ocean. (**A** to **D**) Simulated yellow dye projections of lava-impacted waters overlain on contours of sea surface height. (**E** to **H**) Satellite observations showing the formation and subsequent disappearance of the chlorophyll a plume during June to August 2018.

nitrate supply was not immediately clear. The absence of fixed nitrogen species in mantle-derived magmas means that the lava itself is not a source of nitrate. Yet the strong covariation of nitrate with other lava-derived elements (Fig. 2) implies a mechanistic coupling between lava input and nitrate supply. Chemical fixation of N_2 can occur at temperatures above 1000°C with either O_2 or H_2 as the reactant (*16*, *17*), enhanced by the abundance of metal catalysts derived from the lava. However, this process would result in nitrate with $\delta^{15}N\text{-}NO_3^-$ values of ~0 ± 4‰ (*17*), rather than the $\delta^{15}N\text{-}NO_3^-$ of 9.4 ± 1.3‰ measured here. Groundwater discharge is an alternative source of high concentrations of nitrate to nearshore waters of the Hawaiian Islands (*18*, *19*). However, the isotopic composition of nitrate in local groundwater (*18*) does not overlap with our measurements (Fig. 4A), and salinity anomalies expected from enhanced groundwater flow were not detected within the plume.

We instead hypothesize that injection of lava below the euphotic zone created buoyant plumes of nutrient-rich deep water bringing nitrate to the surface (Fig. 4B). Prior measurements of nitrate isotopic composition at depths of 300 m have $\delta^{15}N\text{-}NO_3^-$ values of 6 to 7‰ and $\delta^{18}O\text{-}NO_3^-$ values of 3‰ (*20*, *21*) (fig. S9). This isotopic composition is consistent with a nitrate source to surface plume waters that subsequently underwent nitrate assimilation, leading to a 1:1 enrichment in $\delta^{15}N\text{-}NO_3^-$ and $\delta^{18}O\text{-}NO_3^-$ (Fig. 4A). Upwelling of waters from below the euphotic zone containing low O_2 would also explain the undersaturation of O_2 in lava-impacted surface waters at the head of the plume (182 μmol kg^{-1} compared to 205 μmol kg^{-1} in non–lava-impacted waters), which is otherwise difficult to account for by biological or abiotic processes alone (table S1 and fig. S10). Historically, much smaller lava ocean-entry events along the Kīlauea coastline were sufficient to create surface "roiling" when the upward motion of water heated by submarine lava intrusions entrained subsurface water (*22*). It is conceivable that the lava flow in summer 2018 reached the mesopelagic environment in the early stages of the phytoplankton bloom, facilitated by the high flow rate and extremely steep offshore bathymetry with water column depths of >300 m less than 1 km offshore. Subsequent remotely operated vehicle observations during September 2018 confirmed that lava intrusions ultimately reached depths of 725 m, and low-temperature venting directly associated with the fresh lava deposits was also observed (*23*). Upwelled waters from this depth would contain sufficient concentrations of nitrate to fuel the observed phytoplankton bloom. After the lava flow substantially decreased on 6 August, the much smaller flow that lasted for an additional month was insufficient to cause buoyant plumes of nutrient-rich deep water.

The large-scale ocean entry of lava during the 2018 eruption of Kīlauea volcano created a large and biologically productive surface plume that was observed hundreds of kilometers offshore and persisted for the duration of the eruption. This strong biological response depended not only on the lava itself but also on an exogenous source of nitrate, which is believed to have derived from lava entering the deep ocean, creating buoyant plumes of nitrate-rich deep water into the nitrogen-starved surface ocean. It is possible that this mechanism has led to similar ocean fertilization events in the past, associated with the formation of the Hawaiian Islands and other major volcanic eruptions. Although greater by a factor of 10 than mean lava production rates at Kīlauea over the past 50 years (*1*), the magnitude of the 2018 eruption (~0.8 km^3) only represents lower-bound estimates of lava production rates during the formation of the Ontong-Java Plateau and other large igneous provinces (1 to >20 km^3 per year) that occurred over thousands to millions of years (*24*, *25*). Such major volcanic episodes coincide with the rapid release of carbon dioxide, global warming, and stratification of the deep ocean (*26*). Depending on their location, sustained eruption on this scale could also facilitate a large flux of nitrate from the mesopelagic ocean and perturb regional ocean circulation and biogeochemistry. Marine ecosystem responses to such substantial additions of nitrate are rarely observed or sampled in real time. The expedition in July 2018 provided a unique opportunity to see first-hand how a massive input of exogenous nutrients alters marine ecosystems attuned to oligotrophic conditions.

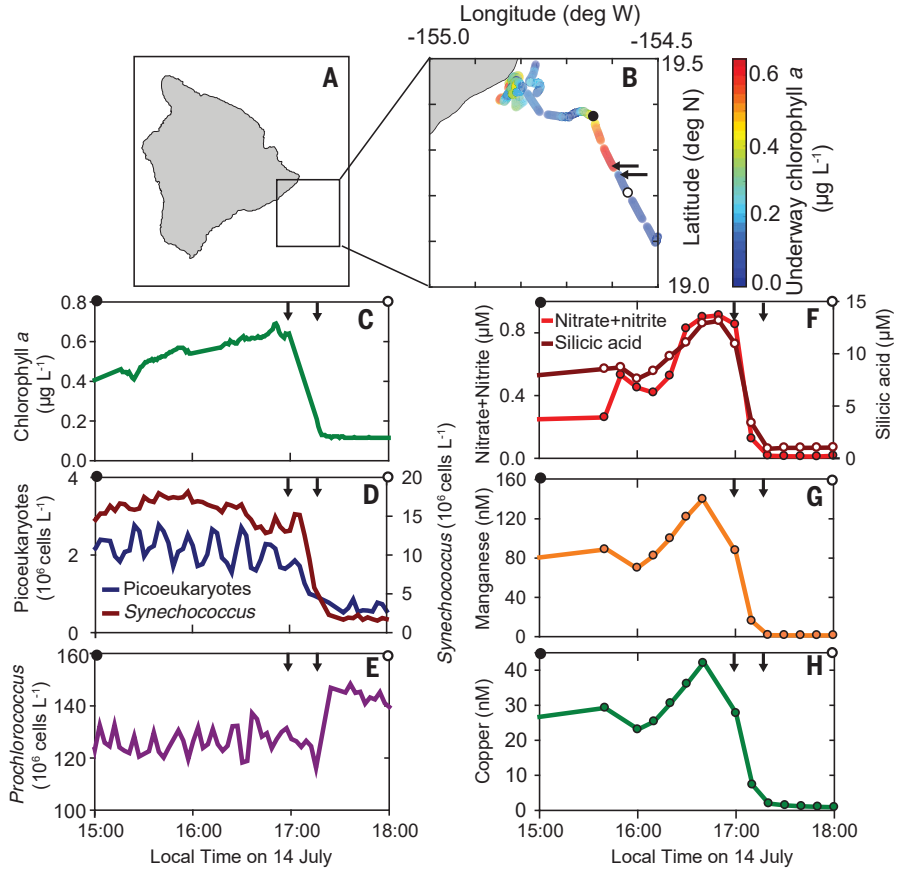

Fig. 2. Transition from lava-impacted waters to the oligotrophic ocean. (**A**) Map of Hawai'i showing sampling location. (**B**) Cruise track depicted by chlorophyll a concentrations. The location of the transition zone (approximately 2 km in length) is marked by the two arrows; the circles indicate the beginning and end of the datasets shown in (C) to (H). (**C** to **H**) The changes in water column properties from the lava-impacted waters (solid circle) to oligotrophic conditions (open circle) are shown for chlorophyll a (C), *Synechococcus* and picoeukaryotes (D), *Prochlorococcus* (E), nitrate + nitrite and silicic acid (F), total dissolvable manganese (G), and total dissolvable copper (H).

REFERENCES AND NOTES

1. C. A. Neal *et al.*, *Science* **363**, 367–374 (2019).
2. U.S. Geological Survey Hawaiian Volcano Observatory, "Preliminary analysis of the ongoing Lower East Rift Zone (LERZ) eruption of Kilauea Volcano: Fissure 8 Prognosis and Ongoing Hazards" (Cooperator Report to Hawaii County Civil Defense, 15 July 2018); https://volcanoes.usgs.gov/vsc/file_mngr/file-185/USGS%20Preliminary%20Analysis_LERZ_7-15-18_v1.1.pdf.
3. K. Govindaraju, *Geostand. Newsl.* **18**, 1–158 (1994).
4. J. A. Resing, F. J. Sansone, *Geochim. Cosmochim. Acta* **66**, 1925–1941 (2002).
5. R. A. Feely *et al.*, *Geochim. Cosmochim. Acta* **60**, 2297–2323 (1996).
6. Y. Li, H. Keppler, *Geochim. Cosmochim. Acta* **129**, 13–32 (2014).
7. J. J. Cullen, *Annu. Rev. Mar. Sci.* **7**, 207–239 (2015).
8. L. Campbell, H. A. Nolla, D. Vaulot, *Limnol. Oceanogr.* **39**, 954–961 (1994).
9. H. Alexander *et al.*, *Proc. Natl. Acad. Sci. U.S.A.* **112**, E5972–E5979 (2015).

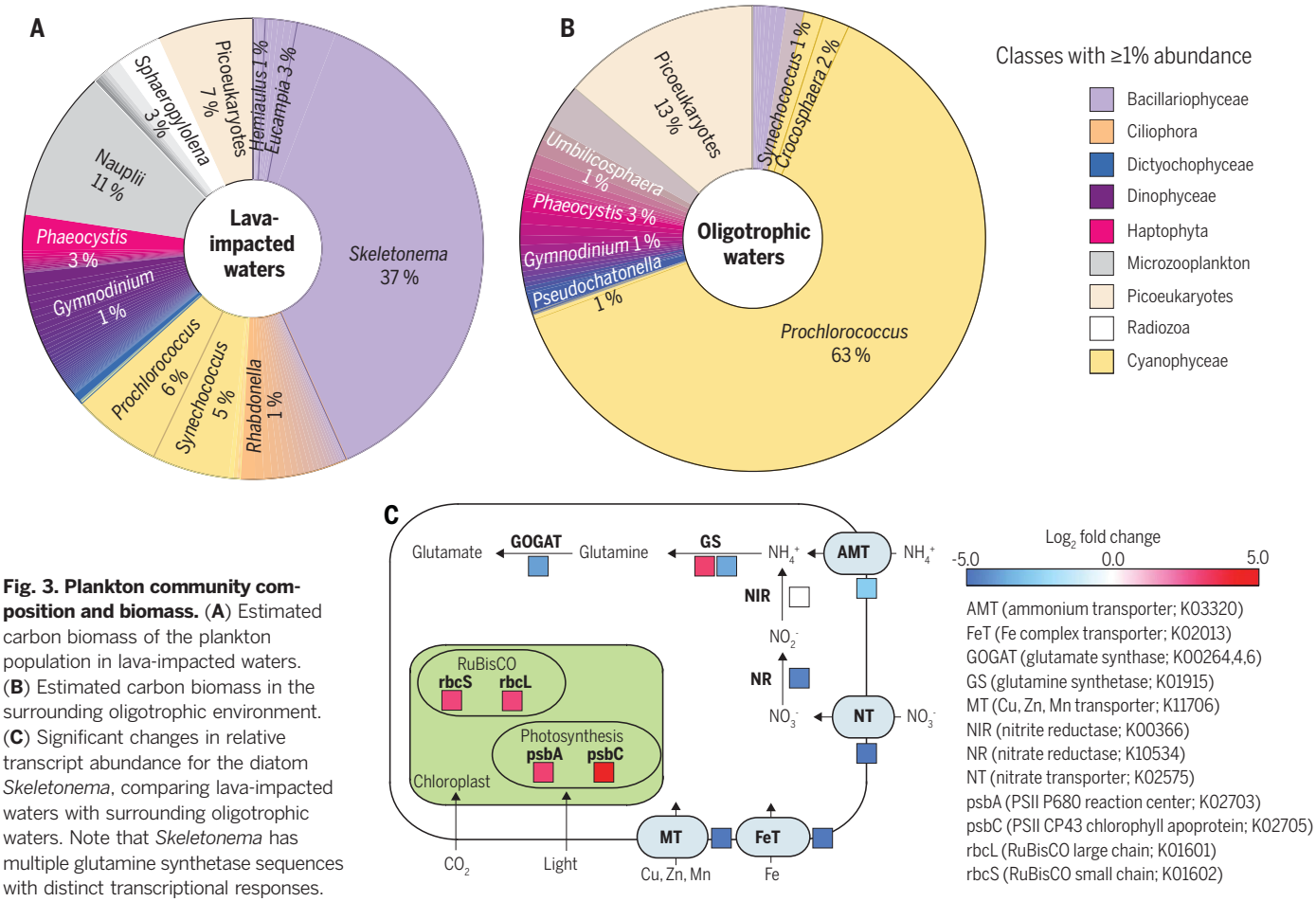

Fig. 3. Plankton community composition and biomass. (**A**) Estimated carbon biomass of the plankton population in lava-impacted waters. (**B**) Estimated carbon biomass in the surrounding oligotrophic environment. (**C**) Significant changes in relative transcript abundance for the diatom *Skeletonema*, comparing lava-impacted waters with surrounding oligotrophic waters. Note that *Skeletonema* has multiple glutamine synthetase sequences with distinct transcriptional responses.

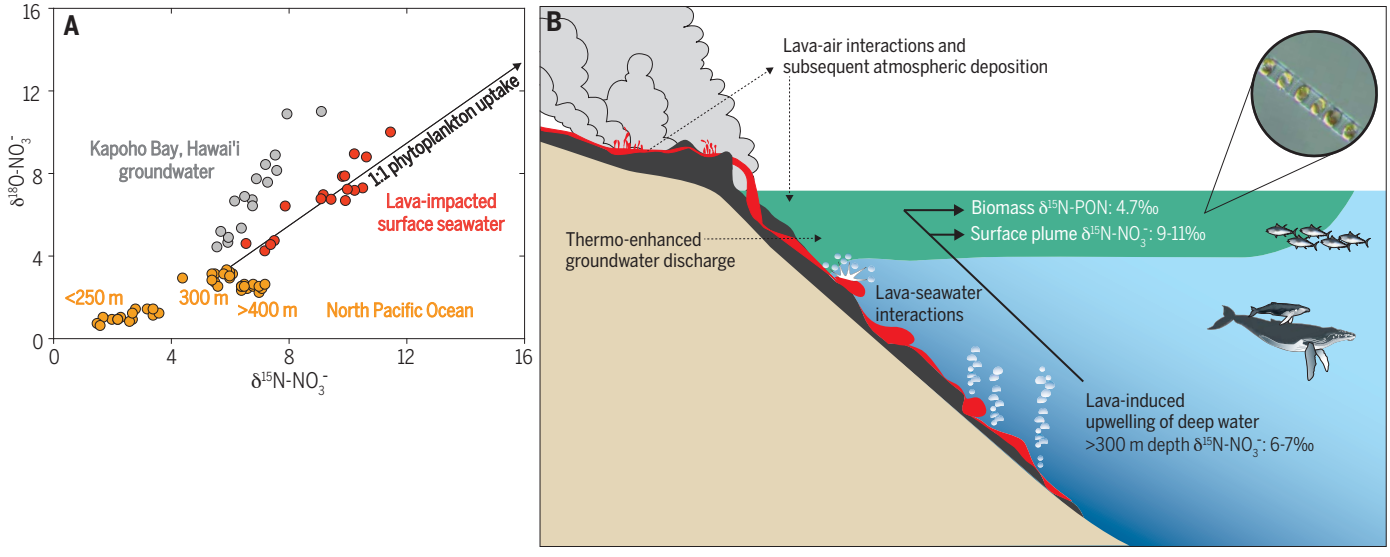

Fig. 4. Nitrate origins. (**A**) $\delta^{15}N\text{-}NO_3^-$ and $\delta^{18}O\text{-}NO_3^-$ along the lava-impacted surface plume waters (red circles) compared with regional subsurface values (yellow circles) (*20*) and local groundwater values (gray circles) (*18*). The line originating from 300 m $\delta^{15}N\text{-}NO_3^-$ follows a trajectory consistent with an isotope effect of 5‰ for NO_3^- assimilation, which would elevate $\delta^{15}N\text{-}NO_3^-$ and $\delta^{18}O\text{-}NO_3^-$ equally (i.e., a slope of 1). (**B**) Schematic of potential nitrate sources during the 2018 eruption, including upwelling of ≥300 m subsurface water, near-shore groundwater discharge, and abiotic N_2 fixation. Partitioning of upwelled nitrate into an isotopically lighter pool of particulate nitrogen and an isotopically heavier pool of residual surface nitrate is highlighted as the most direct explanation of the observations.

10. R. T. Barber, M. R. Hiscock, *Global Biogeochem. Cycles* **20**, GB4S03 (2006).
11. D. M. Karl, R. M. Letelier, *Mar. Ecol. Prog. Ser.* **364**, 257–268 (2008).
12. C. L. Follett, S. Dutkiewicz, D. M. Karl, K. Inomura, M. J. Follows, *ISME J.* **12**, 1543–1557 (2018).
13. S. J. Bender, C. A. Durkin, C. T. Berthiaume, R. L. Morales, E. Armbrust, *Front. Mar. Sci.* **1**, 3 (2014).
14. M. J. Harke, A. R. Juhl, S. T. Haley, H. Alexander, S. T. Dyhrman, *Front. Microbiol.* **8**, 1279 (2017).
15. J. Granger, D. M. Sigman, J. A. Needoba, P. J. Harrison, *Limnol. Oceanogr.* **49**, 1763–1773 (2004).
16. B. Huebert *et al*., *Biogeochemistry* **47**, 111–118 (1999).
17. J. H. Carrillo, M. G. Hastings, D. M. Sigman, B. J. Huebert, *Global Biogeochem. Cycles* **16**, 24-1–24-16 (2002).
18. T. N. Wiegner, A. U. Mokiao-Lee, E. E. Johnson, *Mar. Pollut. Bull.* **103**, 63–71 (2016).
19. J. M. Bishop, C. R. Glenn, D. W. Amato, H. Dulai, *J. Hydrol. Reg. Stud.* **11**, 194–218 (2017).
20. K. L. Casciotti, T. W. Trull, D. M. Glover, D. Davies, *Deep-Sea Res.* **55**, 1661–1672 (2008).
21. A. N. Knapp, D. M. Sigman, F. Lipschultz, A. B. Kustka, G. Capone, *Global Biogeochem. Cycles* **25**, GB4004 (2011).
22. F. J. Sansone, J. A. Resing, *J. Geophys. Res. Oceans* **100**, 13555–13569 (1995).
23. C. R. German *et al*., Time series study of hydrothermal venting at Lō'ihi Seamount following the 2018 Kīlauea eruption. *EOS Trans. Am. Geophys. Union* (abstr.), V14A-07 (2018).
24. S. E. Bryan *et al*., *Earth Sci. Rev.* **102**, 207–229 (2010).
25. M. F. Coffin, O. Eldholm, *Geology* **21**, 515–518 (1993).
26. P. B. Wignall, *Earth Sci. Rev.* **53**, 1–33 (2001).

ACKNOWLEDGMENTS

The dataset presented here resulted from the efforts of many individuals who contributed to the success of the KOK1806 expedition. We thank T. Clemente, S. Poulos, H. Ramm, B. Watkins, G. Foreman, O. Sosa, and A. Vislova for assistance with cruise planning and onboard activity. L. Fujieki processed the hydrographic data, D. Sadler analyzed DIC samples, and K. Babcock analyzed particulate Si and low-level nitrogen. The altimetry and wind products were obtained from the Copernicus Marine and Environment Monitoring Service (CMEMS) (http://marine.copernicus.eu) and the remote chlorophyll images were obtained by MODIS (https://giovanni.gsfc.nasa.gov and https://modis.gsfc.nasa.gov). The GlobColour data (http://globcolour.info) used in this study were developed, validated, and distributed by ACRI-ST, France. We appreciate comments from C. German (Woods Hole Oceanographic Institution) and University of Hawai'i colleagues including F. Sansone, B. Hubert, H. Dulai, and S. Rowland. **Funding:** Supported by Simons Foundation grants 329108 (D.M.K., E.F.D., E.V.A., S.T.D., M.J.F., A.E.I., A.E.W., J.P.Z., S.J.), 574495 (F.R.), and 602538 (N.H.); Gordon and Betty Moore Foundation grant 3794 and the Balzan Prize for Oceanography (D.M.K.); and NSF grants OCE-1842012 (D.M.K. and E.F.D.), OCE-1756524 (S.T.W.), and OCE-1537314 (A.N.K.). The modeling component was supported by NASA grant 80NSSC17K0561 (O.J., S.D., and C.N.H.). **Author contributions:** D.M.K. and E.F.D. initiated expedition planning and implementation. R.M.L. provided satellite observations. S.T.W. led the expedition and post-cruise organization. N.J.H., R.L.K., and S.J. led the trace elemental measurements. M.D. and A.E.W. led the underway optics, IFCB, and chlorophyll measurements. E.M.S. operated the SeaFlow. F.R., A.M.H., and G.V.H. processed and curated the data. M.B., S.F., K.M.B., and S.T.W. conducted the rate measurements including ^{18}O-GPP, ^{14}C assimilation, microbial respiration, and nitrogen fixation. R.K.F., C.P.F., and K.M.B. led the nutrient analyses. T.J.B., R.T., and J.R.C. led the majority of the water column biogeochemical sampling. A.N.K. analyzed the nitrate isotopes. M.J.H. and S.T.D. measured the eukaryote metatranscriptomics. A.K.B. and A.E.I. measured the metabolites. S.D., O.J., M.J.F., and C.N.H. conducted the MITgcm, DARWIN, and OSCAR modeling. K.A.T.-K., B.A.H., and J.P.Z. measured *nifH* abundances. B.B. analyzed the SeaGlider data. S.T.W. and N.J.H. co-wrote the manuscript with contributions from all authors. **Competing interests:** The authors declare no competing interests. **Data and materials availability:** Data and pertinent methodologies are provided in the supplementary materials. The hydrographic and biogeochemical datasets are freely available online at http://scope.soest.hawaii.edu. The eukaryote metatranscriptomic sequence data are deposited in the Sequence Read Archive through the National Center for Biotechnology Information under accession number PRJNA529177.

SUPPLEMENTARY MATERIALS

science.sciencemag.org/content/365/6457/1040/suppl/DC1
Materials and Methods
Supplementary Text
Figs. S1 to S11
Table S1
Movie S1
Data S1 to S3
References (*27*–*59*)

5 April 2019; accepted 17 July 2019
10.1126/science.aax4767